Structural study of amorphous hydrogenated and unhydrogenated titanium carbide thin films by extended x-ray-absorption fine structure and extended electron-energy-loss fine structure

Alain E. Kaloyeros, Wendell S. Williams, Frederick C. Brown,
Alex E. Greene, and John B. Woodhouse
Department of Physics and Materials Research Laboratory, University of Illinois at Urbana-Champaign, Urbana, Illinois 61801
(Received 7 April 1987; revised manuscript received 22 June 1987)

Thin films of hydrogenated and unhydrogenated titanium carbide, known to be amorphous from x-ray and electron diffraction studies, nevertheless exhibit short-range order at the level of the first-nearest-neighbor shell when studied by extended x-ray-absorption fine structure and extended electron-energy-loss fine structure. This short-range order appears to consist of the same octahedrally coordinated units present in crystalline titanium carbide (NaCl structure), where a titanium atom is surrounded by an octahedron of six carbon atoms and vice versa. The persistence of this basic structural unit is attributed to the difference in atomic radii between C and Ti and to the strong nature of the Ti—C bond. A slight relaxation in interatomic distance relative to the crystalline state, which increases upon hydrogenation, is also observed. The atomic positions in the first coordination shell in amorphous titanium carbide are slightly displaced relative to the crystalline form. Yet, upon hydrogenation, this displacement decreases in the first shell, made of carbon atoms and vacancies, surrounding a Ti atom by 40% for the 4.5 at. % H and 60% for the 6 at. % H relative to the unhydrogenated amorphous TiC_x films. By contrast, the structural disorder in the first shell of Ti atoms surrounding a C atom is practically unaffected by the addition of hydrogen. These results imply that the hydrogen atoms, instead of occupying tetrahedral vacancies, fill carbon vacancies in the amorphous phase as they do in crystalline TiC_x, in agreement with our previous findings from static secondary-ion mass spectroscopy and x-ray photoelectron spectroscopy.

I. INTRODUCTION

In this paper, we report on the first structural study of amorphous and crystalline titanium carbide thin films by the combination of extended x-ray-absorption fine structure (EXAFS) and extended electron-energy-loss fine structure (EXELFS).

In its crystalline form—the rocksalt structure, in which carbon atoms occupy the octahedral interstices of the face-centered-cubic sublattice of metal atoms—titanium carbide is a semimetallic ceramic, combining high melting temperature, great hardness, electronic conductivity, and remarkable chemical stability.[1] It is also characterized by a lack of stoichiometry, accommodated by carbon lattice vacancies: the carbon-to-titanium ratio x ranges from 0.50 to 0.97.[2] These metalloid vacancies in TiC_x play a major role in controlling its physical properties.[3] Because it combines such interesting properties, crystalline titanium carbide has aroused great technological interest and is presently being considered for further applications as a protective coating under extreme chemical, thermal, and mechanical conditions. Both in Japan in the United States, titanium carbide has been identified as a candidate material for the "first wall" coating for the fusion reactor.[4] Titanium carbide is also being studied as a low-friction thermal barrier coating for cylinder walls in the adiabatic diesel engine.[5]

On the expectation that the properties of crystalline titanium carbide might be further enhanced by preparing it in amorphous rather than crystalline form, we successfully synthesized hydrogenated and unhydrogenated amorphous titanium carbide thin films by a new technique, namely low-temperature metalorganic chemical-vapor deposition (MOCVD).[6–12] Our investigations showed that titanium carbide in this novel form exhibits properties which are as complex, and in some cases even more interesting—e.g., greater stability in sulfuric acid—than its crystalline counterpart, and which offer new challenges to basic and applied research.[12–14] A major challenge is to identify the structural arrangements of atoms in amorphous titanium carbide films—an essential prerequisite for developing a detailed understanding of its physical and chemical properties.

Determination of the structure of a solid is a difficult task when there is no periodicity.[15] Classical diffraction techniques, which have been successful in structural studies of crystals, produce little helpful information on amorphous TiC_x owing to the lack of translational symmetry. Other experimental procedures yield results averaged over the whole sample.[16] Fortunately, although long-range order does not exist in amorphous materials, they cannot be regarded as structureless at the atomic level.[17] In fact, chemical (or geometrical) short-range order (SRO) exists locally,[18] and special experimental techniques need to be used to investigate this

SRO. One such technique, applied successfully in our studies, consists of combining information from two distinct, direct probes of structure: EXAFS and EXELFS.

EXAFS is the oscillatory modulation of the absorption coefficient on the high-energy side of an x-ray-absorption edge of a constituent atom in a material.[19] The EXAFS oscillations are a final-state photoelectron effect arising from interference between the outgoing photoejected electron wave and the backscattered waves from neighboring atomic sites.[20] In the simple single-scattering approximation—using the formulation of Stern, Sayers, and Lytle[21]—the EXAFS modulations $\chi(k)$ are described by the equation

$$\chi(k)=\frac{\mu(k)-\mu_0(k)}{\mu_0(k)}=\sum_j \frac{N_j A_j(2k)}{kR_j^2} e^{-2k^2\sigma_j^2} e^{-2R_j/\lambda} \times \sin[2kR_j+\delta_j(k)] , \quad (1)$$

where $\mu(k)$ is the total absorption coefficient measured above the edge and $\mu_0(k)$ is the smoothly varying atomic contribution. The summation is over coordination shells of atoms surrounding the absorbing atom, with N_j (the coordination number) atoms in shell j situated at an average distance R_j from the central atom. The first exponential term containing σ_j^2 is a Debye-Waller-type term; however, σ_j^2 is not the usual mean-square vibrational amplitude of an atom, but rather the mean-square relative positional displacement of the central and backscattering atoms from both thermal disorder and structural disorder. The quantity λ is the phenomenological mean free path that corresponds to a finite lifetime of the excited state, $A_j(2k)$ is the backscattering amplitude of the atoms in the jth shell, and $\delta_j(k)$ is the phase shift experienced by the photoelectron as it traverses the potential of the central and backscattering atoms. The variable k is the ejected photoelectron wave vector, which is related to the energy E of the incident photon by $k=[2m(E-E_0)/\hbar^2]^{1/2}$, where m is the electron mass and E_0 is the inner potential or threshold energy caused by the atomic potentials. E_0 represents the reference energy for the kinetic energy of the photoelectron. A factor of $3\cos^2\theta_j$, where θ_j is the angle that the jth neighbor makes with the polarization vector of the x ray, has to be included in the summation for a single-crystal specimen. This factor averages out to 1 for polycrystalline and amorphous materials, as in our studies.

In the form given by Eq. (1), the resultant EXAFS is a sum of sine waves with periods $2kR_j$ from each shell j with an amplitude which represents the number of neighbors modified by an envelope due to the backscattering amplitude, the Debye-Waller-type damping, and the mean-free-path damping.

Equation (1) is valid only for Gaussian-shaped disorder and needs to be modified for more general types of disorder.[22] For the amorphous a-TiC_x and a-TiC_x:H_y systems that we examined, however, the simple form of Eq. (1) is adequate.

As a structural tool, EXAFS spectroscopy has capabilities which not only overlap and complement but also extend the features provided by x-ray and neutron diffraction, Raman spectroscopy, and other structural spectroscopies.[23] By contrast to Raman scattering and other optical techniques,[24] EXAFS provides direct, quantitative details of the local atomic environment around each kind of atom, including the type and number N_j of surrounding atoms, their mean distances R_j, and the dynamic (thermal) and static (structural) displacement σ_j^2 about their averaged positions.[25] Furthermore, EXAFS, in its capacity to perform an absolute determination of the coordination number N_j, is more advantageous than diffuse x-ray scattering, for which such information is density dependent.[26] In one respect, however, EXAFS is complementary to diffuse x-ray scattering: EXAFS gives better resolution on the sharp features in the radial distribution function (RDF) for high-k values (>3 Å^{-1}), whereas diffuse x-ray scattering gives similar information on the slowly varying part of the RDF that is normally unavailable in EXAFS (Ref. 23) due to lack of information below 3 Å^{-1}. Finally, the most advantageous feature of EXAFS, when applied to amorphous systems, is perhaps that, unlike x-ray and neutron diffraction, EXAFS does not depend on long-range order in the solid. Hence, aperiodic systems can be studied with the same ease as crystalline materials.[23,26]

Diffraction techniques detect long-range order and isolate the unit of periodicity.[20] To obtain additional information about the arrangement of atoms within the unit cell, additional modeling and structure simulation are needed. This is not an easy task, especially for crystals with a large number of atoms per unit cell, where the number of variables is too large to justify simulation procedures. This difficulty with standard diffraction methods occurs because only the intensity of the diffracted beam is detected, and its phase information is lost.[23] Furthermore, for those forms of condensed matter which have no long-range order, diffraction techniques have only very limited applicability. A diffraction measurement on such aperiodic materials contains information on the sum of two-particle correlation distances for all of the particles combined. When there are many various types of atoms present in the sample, it is practically impossible to separate the contribution of each,[26] except in very special cases.

However, EXAFS is sensitive mainly to short-range order, so it can contribute to the determination of the arrangement of atoms within the unit cell, for periodic systems, and of the local structural arrangement of atoms (SRO), in amorphous materials.[27,28] By tuning x-ray energies to the absorption edge of interest, EXAFS has the ability to probe the short-range order about each type of atom, and to distinguish the type of nearest-neighbor atoms by their backward scattering characteristics. This combination of features makes it feasible to use EXAFS to investigate the two-particle correlation function about each pair of atoms, even in complicated materials composed of many different atoms.[21] In particular, EXAFS is an extremely powerful technique for simultaneous structural investigations of amorphous and crystalline titanium carbide systems.

One problem associated with EXAFS spectroscopy, however, is its limited ability to extract fine-structure information from low-Z elements ($Z<20$), owing to the experimental difficulties encountered at low photon energies[24] (below $\sim$3000 eV). The unavailability of monochromatic radiation of sufficient resolution and intensity in the soft x-ray region limits the use of a rotating anode x-ray source as a laboratory EXAFS facility for structural studies in the spectral region from the carbon K edge at 285 to 3000 eV. This limitation can be overcome by utilizing a synchrotron radiation source, with its appreciably higher beam intensity, but both grating and crystal monochromators are required to cover the whole 280–3000-eV energy range. Another drawback is the necessity of traveling to a synchrotron source.

These problems have encouraged the search for alternative methods for extracting the fine-structure oscillations from low-atomic-number elements. Although a new EXAFS-related x-ray method[29] which relies on measuring the secondary electron yield was successfully applied to light elements, it tends to emphasize surface (rather than volume) contributions from the sample.

Another approach, extended energy-loss fine structure (EXELFS), employs the energetic electron beam of an analytical electron microscope. This method is sensitive to light elements and is not limited to the surface. EXELFS is the modulation in the differential inelastic electron scattering cross section past an ionization edge of a constituent element in a compound.[30] EXELFS, in the case of forward scattering ($k\sim0$, where k is the electron wave vector), has the same physical origins, contains the same kind of information, is described by the same equation [see Eq. (1)], and can be analyzed in the same way as EXAFS, using the formulation of Stern, Sayers, and Lytle.[21]

Yet, in spite of the numerous similarities between the two spectroscopies, EXELFS does provide some major advantages over EXAFS. In contrast to the x-ray-absorption technique, electron scattering data are most easily obtained at energies below 2 or 3 keV, permitting the extraction of fine-structure information from low-atomic-number elements, $5<Z<20$ for the K edge and $20<Z<40$ for the L_{23} edges.[31] The counting rates achievable in this range with high-energy electrons are competitive with those from synchrotron radiation sources. Furthermore, the data gathering time for electron systems is comparable to that of synchrotron sources, and the instrumentation is more accessible and less expensive. Finally, EXELFS gives high spatial resolution—the electron beam can be focused to small areas, with spot sizes of 100×100 Å^2—which permits the study of inhomogeneous samples.[32] These properties were analyzed by Isaacson and Ultaut,[33] who investigated the effectiveness of tunable x-ray sources (EXAFS) and electron beam systems (EXELFS) in performing chemical and structural spectroscopy of matter. They took into account count rates, signal-to-noise ratio, and sensitivity, as well as applicability to different systems. They concluded that if one is interested in spectroscopic information from small concentrations of material in microscopic areas, or from light elements, electron beam systems are preferred because they have a higher detection sensitivity, while if one is concerned with structural details in a statistically averaged sense, or in heavier elements ($Z>20$), photon beam systems are probably superior. Consequently, since EXELFS spectroscopy complements and expands the features displayed by its EXAFS counterpart, the combination EXAFS-EXELFS presents itself as a powerful tool for probing local atomic environments, especially in compounds composed of both light and heavy constituents, such as titanium carbide.

In this paper, the combination EXAFS-EXELFS is employed in one of its earliest applications to perform structural investigations of amorphous a-TiC_x and a-TiC_x:H_y films. Information generated on the static atomic displacements, local structure of both the metalloid (C K edge by EXELFS) and metal (Ti K edge by EXAFS) constituents, and the location of hydrogen and its effect on the short-range order in the films is presented and discussed. The details of the measurements and of sample preparation are summarized in Secs. II and III, respectively. The data are presented and the analysis explained in Sec. IV, a discussion and an interpretation of the results are given in Sec. V, and finally the main conclusions are outlined in Sec. VI.

II. EXPERIMENT

A. Experimental apparatus and data collection techniques

The EXAFS and EXELFS studies were carried out at the Center for the Microanalysis of Materials, Materials Research Laboratory, University of Illinois at Urbana-Champaign.

The EXAFS data (for the Ti K edge) were collected in a laboratory EXAFS system using a Rigaku RU-200 rotating anode tunable x-ray source spectrometer. The high-intensity x-ray source used a molybdenum target (Mo $K\alpha\sim17.4$ eV) capable of photon fluxes of 5×10^7 s^{-1}, achieved at maximum power in a 10-eV bandpass. This source permits laboratory EXAFS to be obtained on a time scale of a few hours, thus minimizing the effect of source instability over extended periods of operation.[34] The beam position was stationary, and higher-order incident x-ray excitations were practically eliminated through an appropriate choice of excitation voltage—below the threshold potential for second- and higher-order harmonics, and through the use of focusing Johansson curved-crystal monochromator to obtain a focused monochromatic beam. The source was operated at 12–13 kV with beam intensities in the 50–70 mA range. In a laboratory EXAFS system, however, additional structure, due to beam instabilities and emission or absorption features from impurities near or on the target, can be introduced by the incident beam. As the information desired is contained in fine structure, it is of particular importance to remove from the data stream any spurious structure, as well as any residual sources of oscillations which may be mistaken for actual EXAFS.[35]

For this purpose, the detection system was made of two detectors, a beam monitor (I_0) detector placed just

ahead of the sample, and a beam detector (I) positioned behind the sample. Difference spectra are thus obtained from a normalized ratio of I_0/I, and this simultaneous measurement of I and I_0 cancels time-dependent fluctuations in the source of mechanical wobble in the apparatus which can produce intensity changes. Finally, in order to minimize thermal vibration effects, which are known to cause not only a smearing out[36] or damping of the EXAFS oscillations but also a reduction in the useful energy range for EXAFS,[37] the samples were mounted, under vacuum, in a GSK Scientific Model 100 EXAFS cold stage, capable of stable operation between 80 and 550 K, and EXAFS spectra were collected with liquid-nitrogen cooling at 80 K.

The experimental apparatus used in our EXELFS measurements (Ti $L_{2,3}$ edges and C K edge) consisted of a Philips EM430 transmission electron microscope equipped with a Gatan model 607 single magnetic-sector, double-focusing electron-energy-loss spectrometer, operated in the energy-filtering mode, and with an EDAX 9100/60 multichannel analyzer minicomputer, equipped with acquisition and display facilities, and used for data gathering and initial processing. The 300-keV electron beam used has the advantage of allowing us to analyze EXELFS in thicker samples than would be possible at lower energies, and to achieve better counting statistics. Energy-loss spectra were obtained in the CTEM (conventional transmission electron microscopy) mode with a current of about 10 μA into a 1-μm-diam probe. Electrons of a given energy loss were selected by a variable width slit and counted using a plastic scintillator (NE100) -photomultiplier (RCA 8575) -discriminator combination which puts out an analog signal to the spectrum monitor, and output pulses which are counted and stored in the EDAX 9100/60 multichannel analyzer operated in the time sequency mode. Multiple sweeps of the spectrum were added together to give a total dwell time of about 3 s per 1-eV channel. Thermal vibration effects were also minimized by mounting the TEM samples in a Philips model PW6591/01 side-energy cold stage and performing EXELFS measurements with liquid-nitrogen cooling at 80 K.

B. Statistical considerations and thickness effects

Since EXAFS and EXELFS constitute small perturbations, typically 1–10 % in relative magnitude, of the change of intensity at the absorption or ionization edge, it is necessary to measure the EXAFS and EXELFS signals with high precision, and good signal counting statistics must be achieved to yield a high signal-to-noise ratio ($>300{:}1$).

In the case of EXAFS measurements, two major considerations must be addressed to achieve high accuracy and high signal-to-noise ratio in determining $\mu x = \ln(I_0/I)$. The first is a choice of optimum μx (i.e., sample thickness) and the second is the apportionment of time in counting I_0 and I, taking into account the fraction of I_0 absorbed by a partially transparent detector—the ion chamber monitor—placed in front of the sample. These parameters, together with the statistical errors and optimum experimental conditions involved in an absorption measurement, were analyzed in detail by Rose and Shapiro.[36] They argued that the measurement of the intensity ratio of two x-ray beams—having the same spectral composition—is essentially a photon-counting problem, and that, consequently, the well-developed statistics of counting apply. By their statistical theory, if the time involved in the measurement is assumed to be fixed, the absorbed thickness that allows the greatest precision in μx is determined entirely by the ratio of the background counting rate to the incident beam counting rate. This "optimum" thickness μx_c was determined by Rose and Shapiro, when the relative background is negligible—which is the case in EXAFS, where the signal-to-noise ratio must be greater than 300 to be ~ 2.6, thus leading to a I/I_0 ratio of about 0.07. The optimum thickness by this criterion is tied up in the product μx_c but can be readily determined if μx_c is known. However, other considerations, which fall under the general category of "thickness effects," make it desirable to use a smaller μx.[38]

Thickness effects in EXAFS have their origin in the fact that even a supposedly monochromatic x-ray source can and does contain wavelengths well away from the central peak. While these may comprise only a small percentage of the incoming x-ray beam, the transmitted beam, after being attenuated by a strong absorption edge, may be dominated by the impurity wavelengths.[39] Other sources of this phenomenon include cracks or holes in the sample, where some fraction of the x rays can pass relatively unaffected by a change in μx, particle-size effects in a powdered sample (and the corresponding thickness effects in thick films), and long tails on the monochromator transmission function.[40] These experimental factors can cause serious amplitude distortions, which might result in up to $\sim 10\%$ reduction in the coordination number,[41] and considerable attention must be given to minimizing them. Special precautions were thus taken to prepare uniform thin films and homogeneous powdered samples, and an optimum thickness and optimum particle size for the films and powdered specimens used were experimentally determined by collecting EXAFS spectra for films and powdered samples of a crystalline TiC_x of various thicknesses and powder sizes, then performing the entire data analysis and comparing the experimentally derived coordination numbers with known values. We found that the best results are achieved for $1.5 < \mu x < 3.0$, corresponding to a film thickness or powder size of 5 to 10 μm.

The second parameter we needed to optimize in EXAFS measurements was the fraction f of I_0 absorbed by the ion chamber monitor. Rose and Shapiro found that, in order to minimize statistical errors, the optimum fraction f of I_0 that the monitor should absorb must be such that $f = 1/1 + e^{\mu x}$, which led to values of f in the range 15–20 % in our EXAFS studies.

In EXELFS spectroscopy, on the other hand, since the extended fine structure above the core edges consists of small intensity modulations ranging in amplitude typically from 10% near the ionization threshold to less

than 1% a few hundred eV higher in energy, statistics are required to be at the 1%—possibly 0.1%—signal-to-noise level.[31] This corresponds in titanium carbide spectra to between 10^4 and 10^6 counts per channel for the typical background intensities preceding the edges. Considering the small probability of exciting the core electrons, it is clearly critical that optimized instrumentation be achieved in order to realize maximum counting rates. For this purpose, we performed a check of the reliability of the counting rates achievable with our system by selecting typical experimental parameters and making use of the standard expression for the count rate of scattered electrons which have been analyzed by a spectrometer and have lost an energy E through core-level excitations:[31]

$$\frac{dN}{dE} = AJN_a t \frac{d\sigma_e}{dE}(E) , \tag{2}$$

where A is the area of the sample exposed to the beam, t is the thickness, N_a is the number density of atoms in the sample, and $d\sigma_e/dE(E)$ the cross section per unit energy loss. We chose an electron beam of 300 keV, which formed a probe on the specimen with a diameter of 1 μm, and a total probe current of 1–5 A. Furthermore, we assumed an electron-energy-loss magnetic sector spectrometer capable of 1 eV resolution and designed to accept electrons scattered inside a semiangle of 10 mrad. For a sample 100 Å thick consisting of amorphous carbon, the K-shell excitation cross section just above the threshold—using the generalized oscillator strength data calculated by Leapman, Rez, and Mayers[40]—was found to be $d\sigma_e/dE \mid_C \sim 10^{-6}$ Å^2 eV^{-1}atom^{-1}, thus leading to a count rate of $dN/dE \mid_C \sim 5\times10^5$ eV^{-1}s^{-1}. Similarly, for a titanium specimen of identical thickness, and for excitations just above the $L_{2,3}$ edges at 455–161 eV, the use of the calculated oscillator strength data[36] yields $d\sigma_e/dE \mid_{Ti} \sim 0.75\times10^{-6}$ Å^{2}eV^{-1} and a corresponding counting rate of $dN/dE \mid_{Ti} \sim 2\times10^5$ eV^{-1}s^{-1}. Both the carbon and titanium spectra therefore required counting times of about 2 s per eV channel at these core edges. However, because of the decreasing cross section above threshold, the average time per channel used was somewhat larger ($\sim$3 s).

Other distortions and inaccuracies are also present in EXELFS spectra and must be accounted for. These are induced by thickness effects, which in this case are attributed to an entirely different mechanism for EXAFS, namely multiple- (plural-) scattering processes that are intrinsic to electron-energy-loss techniques.[41] The current theoretical models for accurate quantitative EELS-EXELFS analysis assume that the transmitted electron beam has only undergone a single inelastic scattering event within the excited volume of the solid. Unfortunately, the preponderance of low-energy plasmon scattering (collective plasmons and other plural-scattering processes involving valence electrons are the most probable excitations) violates the assumption for virtually all solids greater than $\sim$100 nm in thickness, with the problem being accentuated in higher-atomic-number species. These plural-scattering processes tend to induce extra peaks in the spectrum above the edge, too, thus causing possible inaccuracies in EXELFS analysis, and to increase the background intensity relative to the signal and hence degrade the statistics.

We minimized these multiple-scattering effects by limiting the sample thickness to about 1.5λ (where λ is the inelastic mean free path), which required using samples with typical thicknesses in the range 100–200 Å. Moreover, a deconvolution technique[30,41] was applied during the data analysis to remove from the EXELFS spectra any residual structure resulting from plural scattering. The deconvolution process required dividing the energy-loss spectrum into two regions: the low-loss region, containing the zero-loss peak and energy losses to typically 100 eV, and the core-loss intensity region which included the rest of the spectrum. The first region was then used as a deconvolution function or "instrument function" for the second part of the spectrum. Deconvolution was then achieved by "dividing" the Fourier transform of the second area of the spectrum by that of the first, based on the assumption that the measured core-edge intensity $I_N(E)$ is related to the single-scattering intensity $I_S(E)$ and to low-loss spectrum $I_L(E)$ by

$$I_N(E) = I_S(E) ** I_L(E) , \tag{3}$$

where ** denotes a convolution over energy loss. The Fourier transform of $I_M(E)$ is defined as

$$i_M(e) = i_S(e) i_L(e) , \tag{4}$$

where the Fourier transform is denoted by lower case. The single scattering distribution was thus found by dividing the Fourier transforms $I_M(e)$ and $I_L(e)$, and taking the inverse Fourier transform F^{-1}:

$$I_s(E) = F^{-1} i_M(e) i_0(e) / i_L(e) , \tag{5}$$

where we truncated the high-frequency Fourier coefficients which produce noise by reconvoluting with the instrument resolution $I_0(E)$. This isolation of plural scattering required, in an initial step, performing curve fitting to the background intensity preceding the core edge, which was then extrapolated and subtracted over the whole data range. The background curve[30,41] was taken to be a power-law function of the form AE^{-r}, with the parameters A and r being determined by linear least-squares fitting which was made applicable by computing logarithms of the data coordinates.

III. SAMPLE PREPARATION

The amorphous hydrogenated titanium carbide films were produced by metalorganic chemical-vapor deposition (MOCVD) at low temperatures (200–300 °C) and low pressures ($< 10^{-5}$ torr) from the organometallic compound tetraneopentyl-titanium, $[CH_2C(CH_3)_3]_4Ti$, represented as Ti(neopentyl)$_4$. The method used and the subsequent microchemical and microstructural characterization studies preformed on the films have been reported by Kaloyeros, Allocca, Williams, Pollina, and

Girolami elsewhere,[11,13] and are only summarized here. The films were single-phase titanium carbide, a-TiC_x:H_y, with a carbon-to-titanium ratio x ranging from 0.88 to 0.95, and a hydrogen-to-titanium ratio y varying between 0.05 to 0.12. The samples used in our measurements had compositions of a-$TiC_{0.88}$:$H_{0.12}$, a-$TiC_{0.91}$:$H_{0.09}$, and a-$TiC_{0.95}$:$H_{0.05}$. These specimens were deposited on Pyrex glass substrates and had an average thickness of 2 μm. The films were removed from the substrates by etching with hydrofluoric acid and about five layers were plated on transparent adhesive tape to make samples of sufficient x-ray absorption for the EXAFS measurements to be made. For EXELFS data collection, on the other hand, the samples employed were 100-Å-thick single layers deposited on TEM copper grids.

The unhydrogenated amorphous titanium carbide films, a-TiC_x, were obtained by electron beam vaporization (EBV) from single-crystal chips of high-purity titanium carbide onto Pyrex substrates cooled down to liquid-nitrogen temperature.[9] During evaporation, the pressure in the vaporization chamber was kept below 10^{-7} torr. An electron beam of 10 keV with a maximum power rating of 40 kW was employed to deposit a-TiC_x films with an average thickness of 5000 Å. Three samples, with a composition of a-$TiC_{0.88}$, a-$TiC_{0.91}$, and a-$TiC_{0.95}$, were employed in our EXAFS and EXELFS studies after being modified by the methods described in the previous paragraph, except that 15–20 layers on the average were utilized in the EXAFS investigations. These amorphous, hydrogen-free, single-phase titanium carbide films were mainly used to determine where the hydrogen binds in modifying the amorphous structure and its effect on the SRO of the a-TiC_x:H_y films.

In addition to amorphous a-TiC_x:H_y and a-TiC_x specimens, we measured several samples of crystalline titanium carbide. These specimens, in the form of powders of 99.999% purity, were ground and sieved to a 400 mesh size to assure small grain texture, since, for accurate determination of amplitudes, the particle size should be small compared with the x-ray-absorption length to avoid particle-size and other thickness effects (see Sec. II B). These crystalline samples gave us a standard against which to calibrate changes in coordination numbers, structural disorder σ^2, and atomic distances. This approach also minimized any variations in the backscattering amplitude $A_j(2k)$ and the phase shift $\delta_j(k)$ of the Ti and C atoms between the unknowns a-TiC_x:H_y and a-TiC_x and the standard, crystalline TiC_x, since the chemical environment in the latter is expected to be quite similar to that of the unknowns.[42–44]

IV. DATA PROCESSING AND ANALYSIS

Experimentally, the EXAFS and EXELFS spectra appear as low-intensity oscillations (relative to the jump at the absorption or ionization edges) superimposed on the smooth atomic background which decays with increasing energy above the edge. The data reduction must therefore include a determination of the normalized $\chi(k)$ as defined by Eq. (1), Fourier transforming to real space to determine the radial distribution function $F(r)$, and isolation of the single-shell contribution of EXAFS (or EXELFS), before any real data interpretation or structure determination and analysis were performed. The computer programs used for data processing were obtained from the University of Washington EXAFS program library[45] and were modified by the present authors to account for the fact that not only a different set of compounds was being studied but also that information from a different experimental technique (EXELFS) was being analyzed simultaneously with the EXAFS data.[45] The systematic procedure for deducing structure parameters for a substance of unknown structure and a summary of the various steps of the analysis are presented next.

A. Isolation of the oscillatory EXAFS EXELFS from the smooth background—normalization to the edge step

Typical "raw" EXAFS and EXELFS spectra are shown in Fig. 1 (EXAFS of Ti K edge in crystalline TiC) and Fig. 2 (EXELFS for the C K edge and Ti L edges in a-TiC_x:H_y). These data have not been smoothed, normalized, or had any background removed. The figures are only intended to illustrate the excellent signal-to-noise ratio (>300:1) of these data and the quality of the μx (EXAFS) and intensity (EXELFS) spectra achieved from the samples. These excellent signal counting statistics are essential to producing results with error bars of less than 1.5%, as outlined in Sec. V. This accuracy would not have been possible if the experimental data were collected with poor counting statistics.[46–48]

The initial stages of the analysis must deal with the isolation and normalization of the fine structure. The first step is the isolation of the excitation related to a particular edge of interest. This entails performing a first background removal to remove the smooth background due to processes—such as other edges of lower excitation energy, Compton scattering, excitation of collective modes (plasmons), etc.—which are not associated with the edge of interest. For EXAFS data, this background is well described by a linear fit to the data below the edge. This function is extrapolated into the EXAFS region, and subtracted from the data, thus isolating the edge of interest (Ti K edge).

For EXELFS data, a different scheme is followed. Curve fitting to the background intensity preceding the edge is performed by applying a power-law function of the form $f(E)=AE^{-r}$ (as outlined in Sec. I B), and the resultant curve is again extrapolated and subtracted over the whole data range. Then the single-scattering contribution is found by dividing Fourier transforms of the measured core-edge intensity—convolved with the instrumental resolution to minimize high-frequency Fourier coefficients which produce noise—by the low-loss spectrum intensity.

After this first background subtraction, another linear fit is made through the EXAFS and EXELFS data from 50 to 300 eV above each edge and then extrapolated back to the edge, where its value is employed to normalize the spectra.

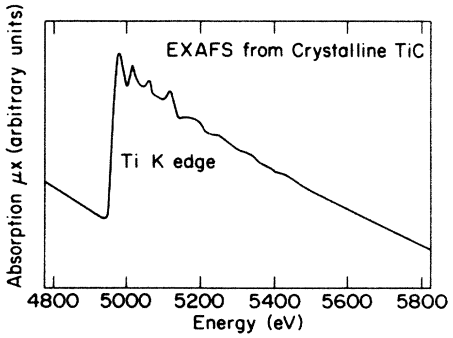

FIG. 1. Typical "raw" x-ray-absorption data, showing EXAFS for the Ti K edge in crystalline TiC. Data have not been normalized, smoothed, or edited.

Following normalization, the data are converted from energy space to electron wave-number k space, where k is defined as $k=[0.263(E-E_0)]^{1/2}$. E is the photon (or incident electron) energy, and E_0 is the effective mean potential experienced by the excited electron. E_0 is taken at this point in the analysis as the energy eV about the first inflection point at the threshold for absorption or ionization.[19,21,23,28] The slowly varying atomic background (second background subtraction) is then removed by fitting a least-squares cubic spline through the data, thus isolating the oscillatory part of the signal from the smooth background.

After removal of the second background, the EXAFS and EXELFS fine-structure modulations are obtained. Figures 3 and 4 show the $\chi(k)$ function, weighted by k^2, for the EXAFS and EXELFS data, respectively, of the Ti K edges and C K edges in all three types of samples (crystalline $TiC_{0.91}$, a-$TiC_{0.91}$, and a-$TiC_{0.91}$:$H_{0.09}$) at 80 K. The weighting scheme (k^n with $n=2$) was chosen so that the relative importance of the various low-k and high-k regions within the data is appropriately emphasized without severely distorting the amplitude envelope.[21,42]

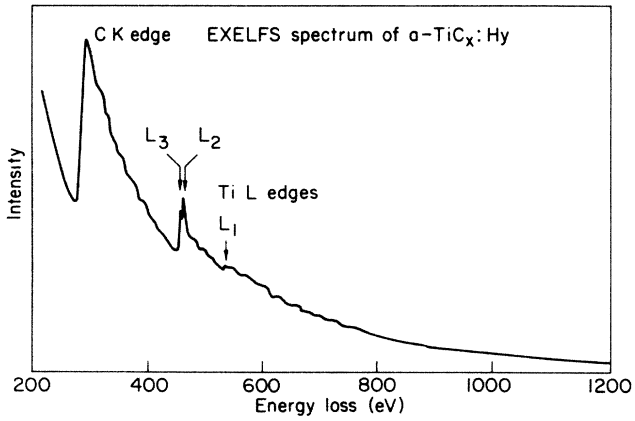

FIG. 2. Typical raw electron-energy-loss data, showing EXELFS past the C K edge and the Ti L edges in a-TiC_x:H_y. Spectra have not been normalized, smoothed, or edited.

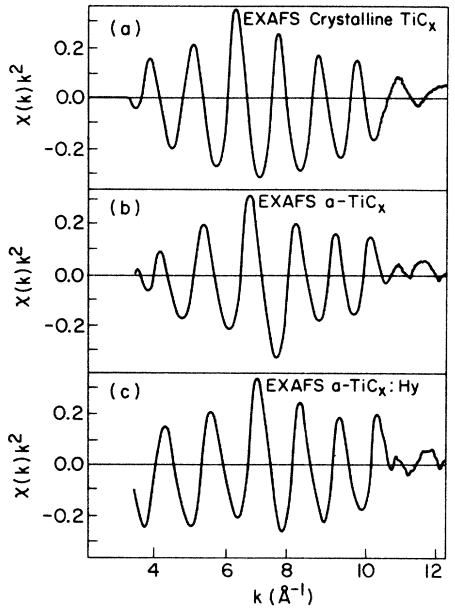

FIG. 3. Isolated EXAFS $\chi(k)k^2$ for the Ti K edge in (a) crystalline $TiC_{0.91}$, (b) a-$TiC_{0.91}$, and (c) a-$TiC_{0.91}$:$H_{0.09}$, all at 80 K.

B. Fourier transforming to a real-space representation

From the EXAFS-EXELFS equation [Eq. (1)], we can see that the fine structure is basically a sum of sinusoidal terms. Consequently, Fourier transforming the data to a real-space representation is a reasonable procedure.[21,38] This step converts the data from a representation in k space to a representation in coordinate space. The latter

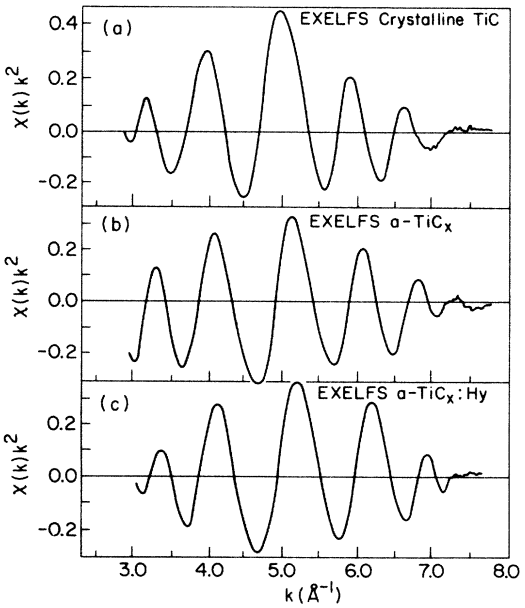

FIG. 4. Isolated EXELFS data $\chi(k)k^2$ at 80 K for the C K edge in (a) crystalline $TiC_{0.91}$, (b) a-$TiC_{0.91}$, and (c) a-$TiC_{0.91}$:$H_{0.09}$.

is known as the radial distribution function, $F(R)$. The peaks in the radial distribution function correspond to the actual interatomic distances shifted by the average slope of the phase shift δ_j,[26] as can be seen from Eq. (1). The peak width will be determined largely by the transform of the amplitude function modulating the oscillations. Clearly, the Fourier transform is an intermediate step which gives an immediate and graphic representation of how many coordination shells contribute to the EXAFS and EXELFS signals and their approximate distances. As displayed in Figs. 5 and 6, the Fourier transform shows that the EXAFS and EXELFS from the amorphous hydrogenated and unhydrogenated samples [Figs. 5(b) and 5(c), and 6(b) and 6(c)] contain only a first-shell signal, while the crystalline titanium carbide spectra show clear contributions from at least three separate coordination shells as well as peaks at higher R that correspond to coordination shells or multiple-scattering paths.[21,23]

C. Isolation of single-shell data by back-transforming the spectra over a restricted R-space window

The Fourier transform is thus an intermediate step which is useful for getting a rough idea of the R-space spectrum and to determine parameters for back-transforming single-shell data to k space. The major reason for backtransforming is the simplicity of determining parameters such as the Debye-Waller factor, coordination number, and distance, by comparing the first-shell signal from the amorphous titanium carbide samples with the crystalline titanium carbide standard. In addition, complications such as nonlinear phase shifts and large structural disorder are usually more easily analyzed in terms of k-space data.

The back-transforming step is a simple extension of the Fourier transform. It is basically an additional Fourier filtering procedure in which the transformed data are inverse transformed over a particular R-space window—in this case an R-space window centered around the peak which corresponds to the first-shell signal—to remove any signals and interferences due to higher-order shells and multiple-scattering processes.[21,38] A representative R-space window is shown in Fig. 7(a) for the EXAFS Ti K edge in crystalline $TiC_{0.91}$, and the result of this filtering is displayed in Figs. 7(b) and 7(c) for the EXAFS Ti K edge and the EXELFS C K edge in crystalline $TiC_{0.91}$.

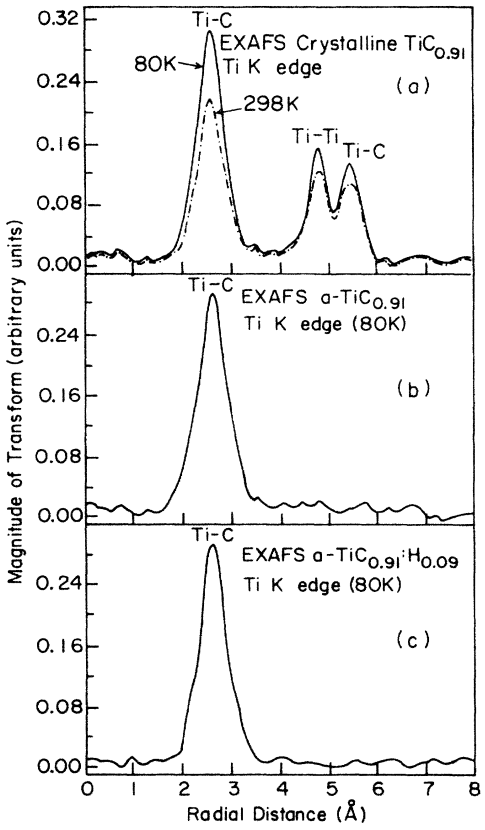

FIG. 5. Fourier transform of EXAFS $\chi(k)$ data from the Ti K edge in (a) crystalline $TiC_{0.91}$ (80 K, 298 K); (b) a-$TiC_{0.91}$ (80 K); and (c) a-$TiC_{0.91}$:$H_{0.09}$.

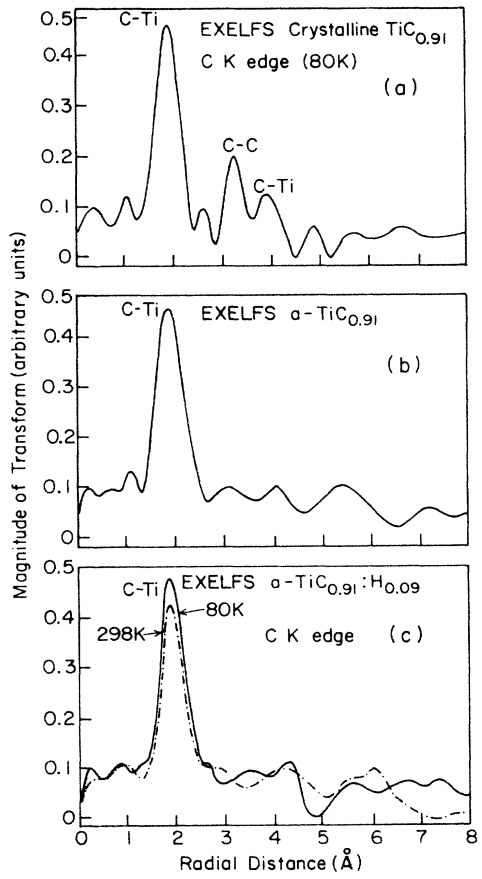

FIG. 6. Fourier transform on EXELFS $\chi(k)$ data from C K edge in (a) crystalline $TiC_{0.91}$ (80 K), (b) a-$TiC_{0.91}$ (80 K), and (c) a-$TiC_{0.91}$:$H_{0.09}$ (80 K, 298 K).

D. Comparison of single-shell data with model compounds using both amplitude and phase information

The structural parameters to be determined are the coordination number, the radial distance to the coordination shell, and the structural disorder σ^2. We proceed by deriving the single-shell EXAFS (or EXELFS) $\chi_1(k)$ for the first shell of the samples with unknown structure, namely a-$TiC_{0.91}$ and a-$TiC_{0.91}$:$H_{0.09}$, and of the standard (crystalline $TiC_{0.91}$). The standard is chosen such that its atomic environment is as similar to the unknown as possible[23,28] to reduce reliance on the assumption of transferability. The next step involves breaking down the single-shell data, shown in Figs. 7(b) and 7(c), into phase and amplitude parts, respectively. As can be seen from Eq. (1), this procedure isolates the distance information R_1 in the phase from the coordination number N_1 and the structural disorder σ_1^2 in the amplitude —where the subscript 1 represents a first-shell information. By computing the phase difference between sample and standard $d\Phi(k)=2(R_s-R_u)k+[\delta_s(k)-\delta_u(k)]$, where the subscripts s and u correspond to standard and unknown, respectively, and plotting it as a function of k, information on the interatomic distance R_u is deduced from the slope of the straight line—which yields twice the difference in interatomic distances, $2(R_s-R_u)$.

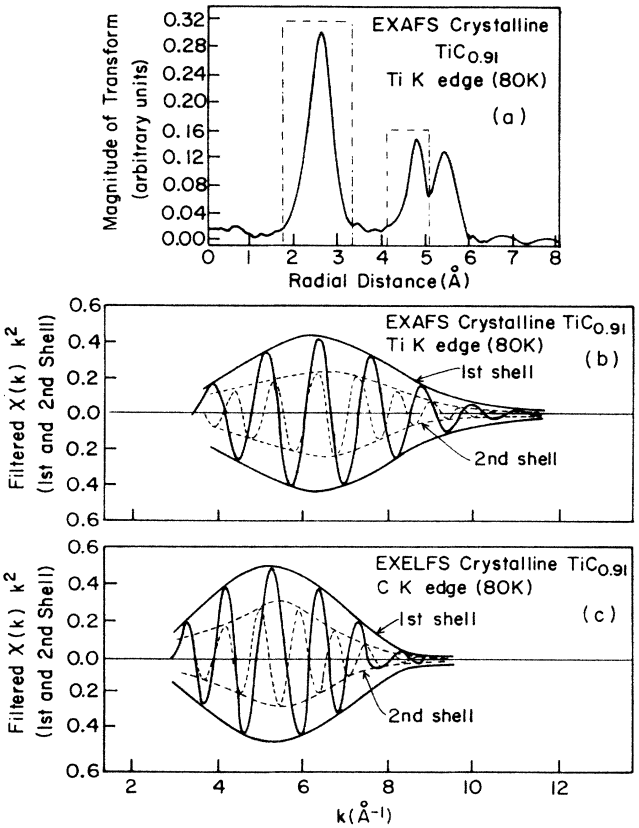

FIG. 7. (a) Typical back-transforming windows for first and second shells in crystalline $TiC_{0.91}$ and (b) single-shell data after back transforming over a limited range in R space using the R windows shown in (a).

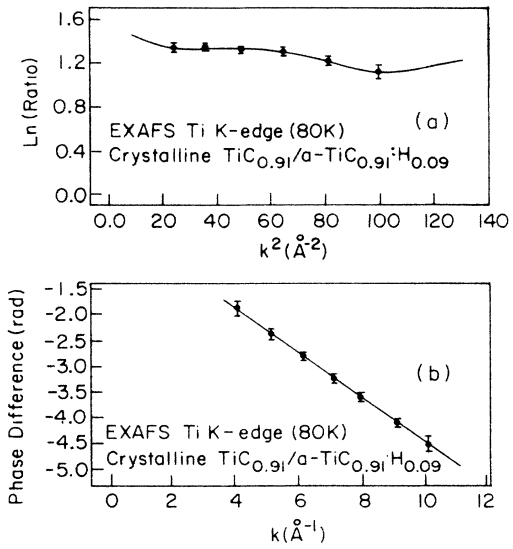

FIG. 8. (a) Natural logarithm of ratio of amplitudes from EXAFS Ti K edge spectra, taken at 80 K, between crystalline $TiC_{0.91}$ and a-$TiC_{0.91}$:$H_{0.09}$ and (b) corresponding phase difference. The relative energy zero between both samples, E_0, has been adjusted by 0.4 eV so that the phase intercept at $k=0$ passes through a multiple of $2n\pi$ (Refs. 23, 38, and 49).

Representative phase difference plots are displayed in Fig. 8(b), for the EXAFS Ti K-edge first-shell phase difference between crystalline $TiC_{0.91}$ and a-$TiC_{0.91}$:$H_{0.09}$, and in Fig. 9(b) for the EXELFS C K-edge first-shell

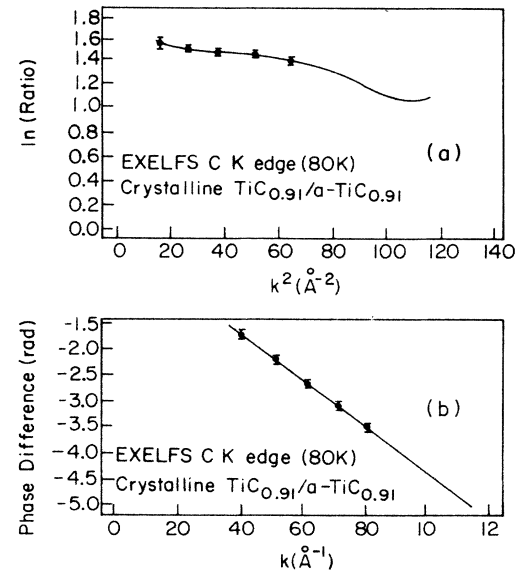

FIG. 9. (a) Natural logarithm of ratio of amplitudes from EXELFS C K-edge spectra, taken at 80 K, between crystalline $TiC_{0.91}$ and a-$TiC_{0.91}$ and (b) corresponding phase difference. The relative energy zero was also adjusted (by ~ 0.6 eV) so that the phase intercept at $k=0$ passes through a multiple of $2n\pi$.

phase difference between crystalline $TiC_{0.91}$ and *a*-$TiC_{0.91}$. Deviations of $d\Phi(k)$ from a straight line, at the high-k end of the spectrum, are due to noise in the data and thermal vibrations. The latter were minimized by comparing phases for the same measurement temperatures (80 K). Other causes of nonlinearity include the failure of the standard EXAFS expression at the low end of the spectrum ($k < 3$ Å^{-1}), and the nontransferability of phase shifts. These deviations can be used to estimate the error in ΔR.

Debye-Waller factors σ_1^2 (structural disorder) and coordination numbers are most easily determined by plotting the natural logarithm of the ratio of the amplitudes of sample and standard versus k^2. The plot of the natural logarithm of the ratio versus k^2 is expected to be a straight line whose slope is twice the structural disorder difference $2\Delta\sigma^2 = 2(\sigma_s^2 - \sigma_u^2)$ and whose intercept is $\ln(N_s R_u^2 / N_u R_s^2)$. Any deviation of this curve from a straight line is an indication of either distortion of the data in the analysis, large non-Gaussian disorder (whether structural or thermal—such as anharmonic thermal effects), or again lack of transferability of amplitude between sample and standard.

Representative natural logarithms of amplitude ratio plots are displayed in Fig. 8(a), for the EXAFS Ti *K*-edge first-shell amplitudes of crystalline $TiC_{0.91}$ and *a*-$TiC_{0.91}$:$H_{0.009}$ and in Fig. 9(a) for the EXELFS C *K*-edge first-shell amplitudes in crystalline $TiC_{0.91}$ and *a*-$TiC_{0.91}$. The error bars in the curves were calculated from two different sources of errors, namely, differences in results obtained from independent analyses of different scans, and deviations in the ratio curves—for both the phase difference and natural logarithm of amplitudes—caused mainly by truncation effects in the Fourier transform, and which are considered as uncertainties in our results. The error bars are larger at the $k_{\min}$ and $k_{\max}$ ends of the spectra because of distortions introduced by truncation effects and Fourier filtering at the lower and upper cutoffs of the data.

Most of the error in the structural determination process is not due to counting statistics or measurement errors, but instead arises from systematics introduced in the analysis process or from inadequacies of the standard EXAFS-EXELFS expression [Eq. (1)], according to Stern and Heald[23] and Teo and Lee.[42] Systematic errors in the analysis include uncertainties in the normalization, relative E_0 determination, and background distortions introduced by the Fourier filtering. We minimized these errors by analyzing the unknowns and standard in exactly the same way and by applying the ratio method, outlined in this section, which tends to make the systematic errors cancel.[21,38] Furthermore, the analysis is greatly simplified by the fact that the types of atoms and the nature of the binding remain almost unchanged between the unknowns (*a*-$Ti_{0.91}$ and *a*-$TiC_{0.91}$:$H_{0.09}$) and standard (crystalline $TiC_{0.91}$), which implies that the backscattering amplitudes, phase shift, and thermal Debye-Waller factors for the Ti and C atoms are expected to show little change in going from crystalline $TiC_{0.91}$ to *a*-$TiC_{0.91}$ to *a*-$TiC_{0.91}$:$H_{0.09}$. Another consequence of this observation is that errors induced by many-body effects tend to cancel.[49,50]

In our work, we started by applying the ratio method (for a detailed description of the ratio method, see Refs. 23, 26, and 43) to the amorphous hydrogenated *a*-$TiC_{0.91}$:$H_{0.09}$ and unhydrogenated *a*-$TiC_{0.91}$ films as compared to crystalline $TiC_{0.91}$ in order to calibrate the first-shell distance, coordination number, and structural disorder σ^2. A subsequent comparison, using the same ratio technique, of *a*-$TiC_{0.91}$:$H_{0.09}$ to *a*-$TiC_{0.91}$ enabled us to isolate structural changes in the amorphous material that are attributable solely to the hydrogen. We also investigated three different levels of hydrogenation to confirm our findings from *a*-$TiC_{0.91}$:$H_{0.09}$. Finally, we have studied the same samples measured at three different temperatures in order to isolate the temperature dependence of σ^2. All the results for the first-shell EXAFS and EXELFS results are summarized in Tables I–III.

V. RESULTS AND DISCUSSION

Before presenting the main results of our analyes, it is necessary to discuss a few topics which deal with the shape and magnitude of the Fourier transform, or radial distribution function $F(R)$, displayed in Figs. 5, 6, and

TABLE I. (a) Results for first-shell EXAFS Ti *K* edge (80 K) for *a*-$TiC_{0.91}$ and *a*-$TiC_{0.91}$:$H_{0.09}$ relative to crystalline $TiC_{0.91}$ and (b) results for first-shell EXELFS C *K* edge (80 K) for *a*-$TiC_{0.91}$ and *a*-$TiC_{0.91}$:$H_{0.09}$ relative to crystalline $TiC_{0.91}$.

Sample	$\Delta N/N$	ΔR (Å)	σ^2 (Å^2)
	(a)		
a-$TiC_{0.91}$	−0.006(10)[a]	0.027(15)[a]	0.001 71(10)[a]
a-$TiC_{0.91}$:$H_{0.09}$	−0.004(15)[a]	0.038(10)[a]	0.001 00(8)[a]
	−0.002(10)[b]	0.009(10)[b]	−0.000 65(10)[b]
	(b)		
a-$TiC_{0.91}$	−0.005(9)[a]	0.019(10)[a]	0.001 89(10)[a]
a-$TiC_{0.91}$:$H_{0.09}$	−0.003(10)[a]	0.032(15)[a]	0.001 33(9)[a]
	−0.006(10)[b]	0.010(10)[b]	−0.000 49(10)[b]

[a]With respect to crystalline $TiC_{0.91}$.
[b]With respect to *a*-$TiC_{0.91}$.

TABLE II. (a) Experimental variation of the mean-square relative displacement $\Delta\sigma^2$ with temperature for EXAFS Ti K-edge nearest-neighbor data for all three types of samples, and (b) differences in $\Delta\sigma^2$ (80 K) between pairs of samples.

Sample	$\Delta\sigma^2$ (10^{-2} Å^2) 80–120 K	80–190 K	80–298 K	80 K
		(a)		
(1) cryst. $TiC_{0.91}$	0.018(10)	0.024(15)	0.051(15)	
(2) a-$TiC_{0.91}$	0.033(15)	0.058(20)	0.108(30)	
(3) a-$TiC_{0.91}$:$H_{0.09}$	0.028(10)	0.045(15)	0.091(20)	
		(b)		
(1)–(2)				−0.015(15)
(1)–(3)				−0.010(10)
(2)–(3)				0.005(5)

7(a), and with the errors compiled for the different structural parameters deduced by EXAFS and EXELFS.

As can be seen in Tables I–III the errors are much smaller than what is typically observed in similar investigations, and it is worthwhile to discuss how this accuracy is achieved. We followed the approach used by Bouldin, Stern, Von Roedern, and Azoulay,[51,52] which consists basically of compiling errors from separate analyses of different scans and comparing structural parameters determined from these scans. Care was also taken to eliminate particle-size and thickness effects and to avoid harmonic contamination in the x-ray beam. In addition, for the absolute calibration of the coordination number change, $\Delta N/N$, and the change in structural disorder factors $\Delta\sigma^2$, three different samples of crystalline $TiC_{0.91}$ were used as standards. The data from these standards were taken at different times on the EXAFS source and the EXELFS TEM microscope for different electron beam energies ranging from 200 to 300 keV, and for x-ray source voltages in the range 12–13 kV. The variations in $\Delta N/N$ and in the structural disorder factors $\Delta\sigma^2$ between these three standards were then determined by the ratio method and included in the error. It was found that $-0.0005 < \Delta N/N < -0.010$, while the change in the structural disorder factor was $\sim 0.000\,07$ to $0.001\,10$ Å^2.

Another observation is that the truncation ripples are more pronounced in the EXELFS than EXAFS data, as seen in Figs. 5 and 6. This effect is attributed mainly to the smaller k range available for analysis in the EXELFS C K-edge spectra. Our studies indicated, however, that accurate structural information can be obtained, despite the limited data range available, if a proper window function is used. This result is in agreement with the findings of Csillag, Johnson, and Stern.[28]

Furthermore, spectra taken at different temperatures (see Figs. 5 and 6 and Tables II and III) exhibit damping effects due to thermal vibrations. This observation agrees with our expectations and with the findings of other researchers[36,37] that thermal vibrations can cause smearing out, or damping, of the EXAFS and EXELFS oscillations as well as a reduction in the useful data range for data analysis (see Figs. 8 and 9). For this reason, all the spectra used for structural determination were collected at liquid-nitrogen temperature (80 K).

Finally, the most important observation in Figs. 5 and 6 is perhaps that the transform contains only a first-shell signal for a-$TiC_{0.91}$ and a-$TiC_{0.91}$:$H_{0.09}$, while crystalline $TiC_{0.91}$ shows clear contributions from at least three separate coordination shells. The Fourier transforms, therefore, not only agree with the present authors' x-ray and electron diffraction (XRD and ED) findings[8,11] on

TABLE III. (a) Experimental variation of the mean-square relative displacement $\Delta\sigma^2$ with temperature for EXELFS C K-edge nearest-neighbor data for all three types of samples and (b) differences in $\Delta\sigma^2$ (80 K) between pairs of samples.

Sample	$\Delta\sigma^2$ (10^{-2} Å^2) 80–170 K	80–220 K	80–298 K	80 K
		(a)		
(1) cryst. $TiC_{0.91}$	0.027(10)	0.032(15)	0.065(20)	
(2) a-$TiC_{0.91}$	0.045(20)	0.081(20)	0.131(25)	
(3) a-$TiC_{0.91}$:$H_{0.09}$	0.035(10)	0.052(15)	0.100(20)	
		(b)		
(1)–(2)				−0.018(15)
(1)–(3)				−0.008(10)
(2)–(3)				0.020 (5)

the amorphicity of the a-$TiC_{0.91}$ and a-$TiC_{0.91}$:$H_{0.09}$ films, they also demonstrate that EXAFS and EXELFS are capable of providing accurate information on the local structure and short-range order (SRO) of the films. The EXAFS and EXELFS results, shown in Figs. 5 and 6, confirm our expectations—attributed to the difference in atomic radii of Ti and C and to the strong covalent nature of the Ti—C bond—that the amorphous phases, whether hydrogenated or unhydrogenated, are not simply formed of random arrangements of Ti and C atoms but include some kind of local short-range order.

Using the ratio method,[26,43,51] we were able to obtain detailed information on the nature, the coordination number, and the interatomic distances of the units involved in the local SRO, as well as on the location of hydrogen in the films and its effect on this SRO. The results follow (see Table I).

1. The EXAFS Ti K-edge and EXELFS C K-edge data show that unhydrogenated a-$TiC_{0.91}$ has, to within experimental error, the same Ti and C coordination number as crystalline $TiC_{0.91}$, very slightly *larger* first-shell interatomic distance, and *larger* structural disorder σ_C^2 and σ_T^2.

2. The EXAFS Ti K-edge and EXELFS C K-edge data show that the addition of hydrogen (in a-$TiC_{0.91}$:$H_{0.09}$) yields the *same* Ti coordination number as a-$TiC_{0.91}$ and crystalline $TiC_{0.91}$. A comparison with both a-$TiC_{0.91}$ and crystalline $TiC_{0.91}$ indicates a slight increase in the titanium interatomic distance for a-$TiC_{0.91}$:$H_{0.09}$ (relative even to a-$TiC_{0.91}$). The hydrogenated sample's static component of σ_{Ti}^2 was larger than crystalline $TiC_{0.91}$ but smaller than its counterpart in the amorphous unhydrogenated films. This implies that a certain degree of order was induced in the first coordination shell (made of C atoms) surrounding a Ti atom in a-$TiC_{0.91}$:$H_{0.09}$ relative to a-$TiC_{0.91}$.

3. From the EXELFS C K-edge data, we note that the carbon in a-$TiC_{0.91}$:$H_{0.09}$ has the *same* coordination number as C in a-$TiC_{0.91}$ and crystalline $TiC_{0.91}$, slightly *larger* interatomic distance and, within experimental error, the *same* structural disorder as a-$TiC_{0.91}$. This result is to be contrasted with the results for Ti in a-$TiC_{0.91}$:$H_{0.09}$, where σ_{Ti}^2 was smaller than that in a-$TiC_{0.91}$, indicating that hydrogenation does not affect the first coordination shell (made of Ti atoms) surrounding a C atom in a-$TiC_{0.91}$:$H_{0.09}$.

VI. CONCLUSIONS

Within the cited errors ($\sim 1.5\%$), these results are consistent and indicate the following.

1. The SRO observed in the amorphous titanium carbide films—both hydrogenated and unhydrogenated—consists of basically the same octahedrally coordinated units observed in crystalline titanium carbide, where a Ti atom is surrounded by six C atoms and vice versa. However, these ordered units are observed at the level of the first coordination shell only in a-$TiC_{0.91}$ and a-$TiC_{0.91}$:$H_{0.09}$. Preliminary modeling indicates that these octahedral units are not space filling.

2. A slight relaxation in interatomic spacings is observed in the amorphous state, and it tends to increase with the addition of hydrogen to the films.

3. The values of the structural disorder σ_{Ti}^2 of a-$TiC_{0.91}$:$H_{0.09}$ are reduced relative to a-$TiC_{0.91}$, while σ_C^2 remains unchanged. This is interpreted as due to the filling of carbon vacancies by hydrogen in the locally ordered octahedral units surrounding a titanium atom, thus reducing the degree of disorder in the corresponding shell. The fact that σ_C^2 remained the same after hydrogenation supports our hypothesis. Furthermore, these results are in agreement with the present authors' findings from x-ray photoelectron spectroscopy (XPS) studies[8,11,53] performed on amorphous hydrogenated films with various degrees of hydrogenation. XPS showed that the hydrogen concentration y was proportional to the number of carbon vacancies $(1-x)$ as for hydrogenated crystalline TiC such as to make the overall composition $x+y\sim 1$, which is as close to stoichiometry as possible. Furthermore, since the H atoms are invisible to EXAFS or EXELFS because of their low backscattering amplitude[23,54] at $k>3$ Å^{-1}, no decrease in coordination is expected in a-$TiC_{0.91}$:$H_{0.09}$ as compared to a-$TiC_{0.91}$. This explains why $\Delta N/N$ was virtually unchanged by hydrogenation (Table III).

4. To confirm our hypothesis concerning the location of H in carbon vacancies of the hydrogenated titanium carbide films, the ratio method was applied to three hydrogenated films with variable degrees of hydrogenation, namely a-$TiC_{0.88}$:$H_{0.12}$, a-$TiC_{0.91}$:$H_{0.09}$, and a-$TiC_{0.95}$:$H_{0.05}$ relative to a-$TiC_{0.88}$, a-$TiC_{0.91}$, and a-$TiC_{0.95}$, respectively. The purpose was to isolate the effect of hydrogen on the structural disorder parameters σ_C^2 (in the local octahedron, made of Ti atoms, surrounding a carbon) and σ_{Ti}^2 (in the local octahedron, made mainly of C atoms, surrounding a titanium). Results showed that in all three cases, $\Delta\sigma_C^2$ (the change in σ_C^2 of a-TiC_x:H_y with respect to the corresponding a-TiC_x) was, within experimental error, virtually the same. However, σ_{Ti}^2 decreased *linearly* with hydrogen concentration increase, from 0.000 94(12) Å^2 for 6 at. % H (i.e., $y=0.12$) to 0.000 65(10) Å^2 for 4.5 at. % H (i.e., $y=0.09$), and finally to 0.000 39(10) Å^2 for 2.5 at. % H (i.e., $y=0.05$). These results are consistent with the findings in Sec. VI, paragraph 3, above and show that the disorder in the locally ordered octahedra around a Ti is reduced in proportion to the increase in hydrogen concentration. Keeping in mind that σ_{Ti}^2 and σ_C^2 are a measure of not only the disorder due to the amorphicity of the films but also of changes in carbon-to-metal ratio x, it becomes clear that hydrogen enters vacancies in the C polyhedra surrounding a Ti atom (as shown by the variations in σ_{Ti}^2, while $\Delta\sigma_C^2\sim 0$), and that it plays a more pronounced role in the films with lower carbon-to-metal ratio.

5. Another possibility is that the H atoms are located in tetrahedral vacancies in the a-TiC_x:H_y structure. This hypothesis is rejected on the grounds that, in this case, one should detect changes in both σ_{Ti}^2 *and* σ_C^2, and that the nearest-neighbor interatomic distance should show a much larger increase than was observed.

ACKNOWLEDGMENTS

This work was supported by the U.S. Department of Energy (Materials Sciences Division), under Contract No. DE-AC02-76ER01198 with the University of Illinois Materials Research Laboratory (MRL). The analyses were carried out in the Center for Microanalysis of Materials of the MRL, which is supported by the U.S. Department of Energy under the same contract number. We thank professional staff members Joyce MacMillan, Peggy Mochel, and Carol Kozlowski for instruction in some of the applied techniques. We also extend our appreciation to the staff of the Coordinated Sciences Laboratory glass shop and the Materials Research Laboratory machine shop, in particular Bill Lawrence, Bud Dittman, and Pat Watson, for their invaluable expertise. We extend our deepest appreciation to Professor Bruce Bunker for his extremely helpful discussions and suggestions.

[1]E. K. Storms, *The Refractory Carbides* (Academic, New York, 1967).

[2]L. E. Toth, *Transition Metal Carbides and Nitrides* (Academic, New York, 1971).

[3]W. S. Williams, in *Progress in Solid State Chemistry,* edited by H. Reiss and J. O. McCaldin (Pergamon, New York, 1971), p. 145.

[4]A. W. Mullendore, J. B. Whitley, H. O. Pierson, and D. M. Mattox, J. Vac. Sci. Technol. **18**, 1049 (1981); M. Okada, Thin Solid Films **108**, 373 (1984).

[5]A. A. Zabolotskii, B. F. Trefilov, N. P. Ignatova, and Y. D. Knot, Sov. Powder Metall. Met. Ceram. **20**, 873 (1982).

[6]R. Morancho, G. Constant, and J. J. Ehrhardt, Thin Solid Films **77**, 155 (1981).

[7]R. Morancho, J. Petit, and G. Constant, J. Electrochem. Soc. **129**, 854 (1982).

[8]A. E. Kaloyeros, M. P. Hoffman, and W. S. Williams, Thin Solid Films **141**, 237 (1986).

[9]A. E. Kaloyeros and W. S. Williams, Surf. Sci. **171**, L454 (1986).

[10]A. E. Kaloyeros and W. S. Williams, Appl. Phys. **A42**, 139 (1987).

[11]A. E. Kaloyeros, C. M. Allocca, W. S. Williams, D. M. Pollina, and G. S. Girolami, Adv. Ceram. Mater. **2**, 100 (1987).

[12]G. S. Girolami, A. E. Kaloyeros, and W. S. Williams, Patent application no. UID 2022 (patent pending); C. M. Allocca, W. S. Williams, and A. E. Kaloyeros, J. Electrochem. Soc. **135**, 3170 (1987).

[13]G. S. Girolami, J. A. Jenson, D. H. Pollina, C. M. Allocca, A. E. Kaloyeros, and W. S. Williams, J. Am. Chem. Soc. **109**, 1579 (1987).

[14]N. G. Odrey, L. Tongson, J. V. Biggers, B. E. Knox, and I. Ham, Thin Solid Films **79**, 83 (1981).

[15]S. R. Elliott, *Physics of Amorphous Materials* (Longman, London, 1983).

[16]*Amorphous Materials: Modeling of Structure and Properties,* edited by V. Vitek (The Metallurgical Society of AIME, Warrendale, Pennsylvania, 1983).

[17]R. Zallen, *The Physics of Amorphous Solids* (Wiley, New York, 1983).

[18]R. Hasegawa, *Glassy Metals: Magnetic, Chemical, and Structural Properties* (CRC, Boca Raton, Florida, 1983).

[19]J. Wong, in *Glassy Metals I: Ionic Structure, Electronic Transport, and Crystallization,* edited by H. Beck and H.-J. Guntherodt (Springer-Verlag, Berlin, 1981), p. 45.

[20]E. A. Stern and J. J. Rehr, Phys. Rev. B **27**, 3351 (1983).

[21]D. E. Sayers, E. A. Stern, and F. W. Lytle, Phys. Rev. Lett. **27**, 1024 (1971); E. A. Stern, Phys. Rev. B **10**, 3027 (1974); F. W. Lytle, D. E. Sayers, and E. A. Stern, *ibid.* **11**, 4825 (1975); and E. A. Stern, D. E. Sayers, and F. W. Lytle, *ibid.* **11**, 4836 (1975).

[22]P. Eisenberger and G. S. Brown, Solid State Commun. **29**, 481 (1979); J. M. Tranquada, in *EXAFS and Near-Edge Structure III,* edited by K. O. Hodgson, B. Hedman, and J. E. Penner-Hahn (Springer-Verlag, Berlin, 1981), p. 74; G. Bunker, Nucl. Instrum. Methods **207**, 437 (1983).

[23]E. A. Stern and S. M. Heald, in *Handbook on Synchrotron Radiation,* edited by E. E. Koch (North-Holland, Amsterdam, 1983), p. 955.

[24]T. M. Hayes and J. B. Boyce, in *Solid State Physics,* edited by H. Ehrenreich, F. Seitz, and D. Turnbull (Academic, New York, 1982), Vol. 37, p. 137.

[25]J. G. Hernandez and R. Tsu, Appl. Phys. Lett. **42**, 90 (1983); R. Tsu, J. G. Hernandez, J. Doehler, and S. R. Oushinsky, Solid State Commun. **46**, 79 (1983).

[26]N. K. Teo, *EXAFS: Basic Principles and Data Analysis* (Springer-Verlag, Berlin, 1986), p. 21.

[27]F. Evangelisti, M. Garozzo, and G. Conte, J. Appl. Phys. **53**, 7390 (1982); R. Frahm, R. Haensel, and P. Rabe, in *EXAFS and Near-Edge Structure,* edited by A. Bianconi, L. Incoccia, and S. Stipcich (Springer-Verlag, Berlin, 1983), p. 107.

[28]S. Csillag, D. E. Johnson, and E. A. Stern, in *EXAFS Spectroscopy: Techniques and Applications,* edited by B. K. Teo and D. C. Joy (Plenum, New York, 1981), p. 241; J. Stohr, R. Jaeger, J. Feldhaus, S. Brennan, D. Norman, and G. Apai, Appl. Opt. **19**, 3911 (1980).

[29]J. Stohr, in *Emission and Scattering Techniques: Studies of Inorganic Molecules, Solids, and Surfaces,* edited by Peter Day (Reidel, Dordrecht, 1981), p. 213; A. S. Vinogradov, E. O. Filatova, and T. M. Zimkina, Fiz. Tverd. Tela (Leningrad) **25**, 1120 (1983) [Sov. Phys.—Solid State **25**, 643 (1983)].

[30]R. F. Egerton, *Electron Energy-Loss Spectroscopy in the Electron Microscope* (Plenum, New York, 1986), p. 224.

[31]R. D. Leapman, L. A. Grunes, P. L. Fejes, and J. Silcox, in *EXAFS Spectroscopy; Techniques and Applications,* edited by B. K. Teo and D. C. Joy (Plenum, New York, 1981), p. 217.

[32]R. D. Leapman, in *Microbeam Analysis–1982,* edited by K. F. J. Heindrich (San Francisco Press, San Francisco, 1982), p. 111; L. A. Grunes, R. D. Leapman, C. N. Wilker, R. Hoffmann, and A. B. Kunz, Phys. Rev. B **25**, 7157 (1982).

[33]M. Isaacson and M. Ultaut, Optik (Stuttgart) **50**, 213 (1978); M. Ultaut, in *EXAFS Spectroscopy: Techniques and Applications,* edited by B. K. Teo and D. C. Joy (Plenum, New York, 1981), p. 255.

[34]G. S. Knapp, H. Chen, and T. E. Klippert, Rev. Sci. Instrum. **49**, 1658 (1978); G. S. Knapp, H. H. Pan, P. Georgopoulos, and T. E. Klippert, in *EXAFS and Near-Edge Structure,* edit-

ed by A. Bianconi, L. Incoccia, and S. Stipcich (Springer-Verlag, Berlin, 1983), p. 402.

[35]G. S. Knapp and P. Georgopoulos, in *Laboratory EXAFS Facilities–1980,* edited by E. A. Stern (AIP, New York, 1980), Chap. 1; E. A. Stern, *ibid.*, Chap. 4.

[36]M. E. Rose and M. M. Shapiro, Phys. Rev. **74**, 1853 (1948).

[37]S. M. Heald and E. A. Stern, Phys. Rev. B **16**, 5549 (1977); E. A. Stern and K. Kim, *ibid.* **23**, 3781 (1981).

[38]B. Bunker, Ph.D. thesis, University of Washington, 1980.

[39]K. Q. Lu and E. A. Stern, Nucl. Instrum. Methods **212**, 475 (1983).

[40]R. D. Leapman, P. Rez, and D. F. Mayers, J. Chem. Phys. **72**, 1232 (1980).

[41]D. C. Joy, R. F. Egerton, and D. M. Maher, Scanning Electron Microsc. **II**, 817 (1979); R. D. Leapman and C. R. Swyt, in *Analytical Electron Microscopy—1981,* edited by R. H. Geiss (San Francisco Press, San Francisco, 1981), p. 164.

[42]B. K. Teo and P. A. Lee, J. Am. Chem. Soc. **101**, 2815 (1979).

[43]E. A. Stern, B. Bunker, and S. M. Healds, Phys. Rev. B **21**, 5521 (1980); J. Stohr, R. Jaeger, and J. J. Rehr, Phys. Rev. Lett. **51**, 821 (1983).

[44]P. A. Lee and G. Beni, Phys. Rev. B **15**, 2862 (1977).

[45]*EXAFS Program Library Manual* (University of Washington, Seattle, Washington, 1981) (unpublished); A. E. Kaloyeros, EXAFS-EXELFS Users Manual (University of Illinois, Urbana, Illinois, 1986) (unpublished).

[46]G. Stegemann and B. Lengeler, J. Phys. (Paris) Colloq. **47**, C8-407 (1987).

[47]B. Lengeler, Z. Phys. B **61**, 421 (1985).

[48]B. Lengeler, in *Disorder Phenomena in Solids (Winterschool 85),* edited by the Institüt für Festkörperforschung der Kernforschungsanlage (Roskilde, Denmark, 1985), p. 225.

[49]D. V. Baxter, in *EXAFS and Near-Edge Structure III,* edited by K. O. Hodgson, B. Hedman, and J. E. Penner-Hahn (Springer-Verlag, Berlin, 1984), p. 77.

[50]G. Bunker and E. A. Stern, Phys. Rev. Lett. **52**, 1990 (1984); N. Alberding and E. D. Crozier, Phys. Rev. B **27**, 3374 (1983).

[51]V. R. Bouldin, E. A. Stern, B. Von Roedern, and J. Azoulay, Phys. Rev. B **30**, 4462 (1984).

[52]C. E. Bouldin, E. A. Stern, B. Von Roedern, and J. Azoulay, J. Non-Cryst. Solids **66**, 105 (1984).

[53]A. E. Kaloyeros, Ph.D. thesis, University of Illinois, 1987.

[54]P. H. Citrin, P. Eisenberger, and B. M. Kincaid, Phys. Rev. Lett. **36**, 1346 (1976).